Biosensors and Bioelectronics 47 (2013) 508–514

Contents lists available at SciVerse ScienceDirect

Biosensors and Bioelectronics

journal homepage: www.elsevier.com/locate/bios

# Simultaneous capture and *in situ* analysis of circulating tumor cells using multiple hybrid nanoparticles

Hun Joo Lee [a,b,1], Hyeon-Yeol Cho [c,1], Jin Ho Oh [d], Kak Namkoong [a], Jeong Gun Lee [a], Jong-Myeon Park [a,e], Soo Suk Lee [a], Nam Huh [a,*], Jeong-Woo Choi [b,c,*]

[a] *In Vitro Diagnostics Lab, Bio Research Center, Samsung Advanced Institute of Technology (SAIT), Samsung Electronics Co., Ltd., Kyunggi-do 446-712, Republic of Korea*
[b] *Interdisciplinary Program of Integrated Biotechnology, Sogang University, Seoul 121-742, Republic of Korea*
[c] *Department of Chemical & Biomolecular Engineering, Sogang University, Seoul 121-742, Republic of Korea*
[d] *Samsung Biomedical Research Institute, Samsung Advanced Institute of Technology (SAIT), Samsung Electronics Co., Ltd., Kyunggi-do 446-712, Republic of Korea*
[e] *Department of Chemistry and Center for Bioactive Molecular Hybrids, Yonsei University, Seoul 120-749, Republic of Korea*

ARTICLE INFO

*Article history:*
Received 12 February 2013
Received in revised form
19 March 2013
Accepted 19 March 2013
Available online 3 April 2013

*Keywords:*
Circulating tumor cell (CTC)
Cell capture
*In situ* analysis
Nanoparticle
Micro-pillar chip

ABSTRACT

Using hybrid nanoparticles (HNPs), we demonstrate simultaneous capture, *in situ* protein expression analysis, and cellular phenotype identification of circulating tumor cells (CTCs). Each HNP consists of three parts: (i) antibodies that bind specifically to a known biomarker for CTCs, (ii) a quantum dot that emits fluorescence signals, and (iii) biotinylated DNA that allows capture and release of CTC–HNP complex to an in-house developed capture & recovery chip (CRC). To evaluate our approach, cells representative of different breast cancer subtypes (MCF-7: luminal; SK-BR-3: HER2; and MDA-MB-231: basal-like) were captured onto CRC and expressions of EpCAM, HER2, and EGFR were detected concurrently. The average capture efficiency of CTCs was 87.5% with identification accuracy of 92.4%. Subsequently, by cleaving the DNA portion with restriction enzymes, captured cells were released at efficiencies of 86.1%. Further studies showed that these recovered cells are viable and can proliferate *in vitro*. Using HNPs, it is possible to count, analyze *in situ* protein expression, and culture CTCs, all from the same set of cells, enabling a wide range of molecular- and cellular-based studies using CTCs.
© 2013 Elsevier B.V. All rights reserved.

## 1. Introduction

As circulating tumor cells (CTCs) may indicate whether a patient has cancer with high likelihood of becoming metastatic, accurate and early detection of CTCs holds great clinical potential, especially in terms of cancer prognosis, diagnosis of minimal residual disease, assessment of tumor sensitivity to drugs, and personalization of anti-cancer therapy (Gerges et al., 2010; Pantel and Alix-Panabières, 2010; Paterlini-Brechot and Benali, 2007; Sieuwerts et al., 2009). Enumeration of CTCs from cancer patients has shown clinical utility in determining the prognosis of metastatic breast, colorectal, and prostate cancers (Ignatiadis and Reinholz, 2011; Kirby et al., 2012). Furthermore, characterization of CTCs using biomarkers has provided pharmacodynamic information for targeted cancer therapy. For example, assessment of HER2 and EGFR expression in CTCs may be potentially predictive in determining personalized anti-cancer therapy (Riethdorf et al., 2010). However, CTCs exist in extraordinarily rare numbers (one CTC per $10^9$ normal cells in blood), making highly efficient and specific capture of CTCs a prerequisite to obtain meaningful clinical information (Yu et al., 2011).

Most CTC capture techniques employ affinity-based positive selection, taking advantage of differences in expression levels of certain surface antigens, which are usually absent in normal leukocytes and erythrocytes (Bednarz-Knoll et al., 2011). One common method of affinity-based selection involves the use of magnetic particles for separation, such as in magnetic activated cell sorting system (MACS), Magsweeper, and CellSearch® (Veridex, Raritan, NJ) (Chung et al., 2011; Lazar et al., 2012; Lin et al., 2011; Talasaz et al., 2009); other methods utilize microfluidic platforms, such as CTC-chip (Nagrath et al., 2007). All affinity-based selections face the same inherent limitation of being

* Co-corresponding authors at: Jeong-Woo Choi: Department of Chemical & Biomolecular Engineering, Sogang University, 35 Baekbeom-ro, Mapo-gu, Seoul 121-742, Republic of Korea. Tel.: +82 2 705 8480; fax: +82 2 3273 0331. Nam Huh: In Vitro Diagnostics Lab, Bio Research Center, Samsung Advanced Institute of Technology (SAIT), Samsung Electronics Co., Ltd., Kyunggi-do 446-712, Republic of Korea. Tel.: +82 31 280 6981; fax: +82 31 280 8277.
*E-mail addresses:* jwchoi@sogang.ac.kr (J.-W. Choi), namhuh@samsung.com (N. Huh).
[1] Equal contribution.

0956-5663/$ - see front matter © 2013 Elsevier B.V. All rights reserved.
http://dx.doi.org/10.1016/j.bios.2013.03.040

completely dependent on the capture antibody used. Many current CTC capture platforms, including CellSearch and CTC-chip, use EpCAM (epithelial cell adhesion molecule) as the sole target antigen, despite reports of EpCAM being expressed in most but not all tumor cells (Cohen et al., 2008; Kumeria et al., 2012). This may be troubling considering that EpCAM is downregulated during the progression of epithelial-to-mesenchymal transition (EMT), in order to promote dissociation of potential future CTCs from tumor mass and invasion into the bloodstream (Gorges et al., 2012; Lin et al., 2012). Moreover, the type and expression levels of surface proteins may vary greatly in CTCs, depending on histological cancer subtype. For example, breast cancers are often divided into five histological subtypes (luminal A/B, HER2, basal-like, and normal-like subtypes), based on protein expression profiles. Cancer cells from basal- and normal-like subtypes show low levels of EpCAM expression (Goldhirsch et al., 2011; Punnoose et al., 2010; Sihto et al., 2011) and are unlikely to be captured by EpCAM alone. Thus, to achieve efficient capture of all CTCs, multiple antibodies should be used in conjunction.

However, CTC capture using multiple antibodies may limit accurate analysis of *in situ* expression of some surface biomarkers, as many candidates for CTC capture are also important markers for CTC characterization. Considering the limited number of known surface proteins specific to each cancer subtype and the extremely rare nature of CTCs, it would be beneficial to perform both positive selection and *in situ* expression analysis by targeting the same maker using a single compound (Zylstra et al., 2012). To solve this challenge, we developed a hybrid nanoparticle (HNP), which consists of three parts: (i) antibodies that bind to specific surface proteins on CTCs, (ii) a quantum dot that emits fluorescence signals upon excitation, and (iii) biotinylated DNA that are used by an in-housed developed, streptavidin-coated chip to capture only CTCs. The DNA linker can also be cleaved post-capture, using restriction enzymes, to recover CTCs from the chip for further use, if necessary.

## 2. Materials and methods

### 2.1. Formation of hybrid nanoparticles (HNPs)

Three different types (emission wavelengths of 525 nm, 565 nm, and 625 nm) of streptavidin-modified quantum dots (Qdots) were purchased from Invitrogen (Carlsbad, CA). Biotinylated antibodies for EpCAM, EGFR, and HER2 were purchased from R&D Systems (Minneapolis, MN). Biotinylated complementary DNA was purchased from Bioneer (Daejeon, Korea) with the following specific recognition sequences:

DNA1: biotin-5'-ATGATAGGAGTAAGCTTGTAAGCTTG-3'
3'-ATCCTCATTCGAACATTCGAACCAG-5'-biotin;
DNA2: biotin-5'-CGACGCTTCGTGGATCCGTGGATCCT-3'
3'-CGAAGCACCTAGGCACCTAGGATCT-5'-biotin;
DNA3: biotin-5'-CACATCATGTAGAATTCTAGAATTCT-3'
3'-AGTACATCTTAAGATCTTAAGACGT-5'-biotin.

Stock solutions of DNA were prepared in deionized water (DW) and kept frozen until use. Each streptavidin-modified Qdot was conjugated to one type of antibody and double stranded DNA (dsDNA). Synthesis of the hybrid nanoparticle (HNP) is shown in Fig. 1. Streptavidin-modified Qdots (2 pmol) were coupled to 1–100 pmol of biotinylated antibodies (0.5:1–50:1 molecular ratio) in 1 × PBS by avidin–biotin reaction (2 h) in dark at room temperature. Subsequently, bi-biotinylated dsDNA (100 pmol) was allowed to react with remaining free streptavidin on the surface of antibody-conjugated Qdots at room temperature (2 h). HNPs were purified by centrifugation (3000*g*, 10 min) to remove large aggregates and filtered to remove excess DNA.

### 2.2. Fabrication of capture & recovery chip

Capture & recovery chip (CRC) was fabricated by silicon-on-glass (SOG) technology to create a precise pillar array structure. Briefly, silicon and glass wafers were bonded using anodic methods. Lapping and chemical mechanical polishing was performed on the silicon layer of the chip, resulting in filter height of 50 μm (determined by the Si layer). Photoresist (AZ 4330, Clariant Corp., Muttenz, Switzerland) was patterned and deep reactive-ion etching was performed (15 min). To make a fluidic path, glass wafer was laminated and patterned using a dry film photoresist (Ordyl BF 410, Tokyo Ohka Kogyo, Kawasaki, Japan), followed by sand blasting etching to form inlet/outlet holes. Finally, the cover glass wafer was aligned and connected with the patterned SOG wafer by anodic bonding

To immobilize streptavidin, CRCs were sequentially rinsed with ethanol and deionized (DI) water and dried at 60 °C overnight. The chips were then placed in a plasma chamber (Convance-MP, Femto Science, Gyeonggi-do, Korea) and exposed to oxygen plasma (5 min) to activate surface silanols for subsequent reaction. The chips were immersed in 10% 3-aminopropyltriethoxysilane (Sigma-Aldrich, MO) solution, thoroughly washed with DI water, and baked at 110 °C for 1 h. The silanized chips were exposed to 2% glutaraldehyde (Sigma-Aldrich) solution in 100 mM phosphate buffer (pH 8.0) for 1 h, washed with PBS, and dried with $N_2$. 10 μM of streptavidin (Sigma-Aldrich) was allowed to react with immobilized glutaraldehyde at room temperature (1 h). After washing with PBS, the chips were covered with 1% bovine serum albumin (Sigma-Aldrich) in PBS (1 h) to block any sites not bound to proteins on the glutaraldehyde-modified surface. Finally, CRCs were washed with PBS solution and dried with $N_2$ (Lee et al., 2009).

### 2.3. Cancer cell culture

Three breast cancer cell lines (MCF-7, MDA-MB-231, and SK-BR-3) were obtained from ATCC (Manassas, VA). All cell culture media and supplements were obtained from Invitrogen (Carlsbad, CA), unless otherwise noted. MDA-MB-231 cancer cell lines were grown in RPMI 1640 media, while MCF-7 and SK-BR-3 cells were grown in Dulbecco's Modified Eagle Medium (DMEM). All media were supplemented with 10% fetal bovine serum (FBS) and 1% penicillin–streptomycin. Cells were grown at 37 °C and 5% $CO_2$ in TC-grade Petri dish (BD Biosciences, San Jose, CA).

### 2.4. Blood sample handling

All healthy human blood samples were obtained from Severance Hospital of the Yonsei University (Seoul, Korea), and this work was approved by the Institutional Review Board (IRB). As CTCs exist in the buffy coat layer, a density gradient reagent (Ficoll-Paque plus, GE Healthcare Inc.) was carefully layered upon whole blood. The upper layer of this reagent, which contains the buffy coat layer, was obtained after centrifugation at 1000*g* for 30 min.

### 2.5. CTC capture using capture & recovery chip

Cell spiking experiments were conducted to test CTC capturing capabilities of CRC. 1 pmol of HNPs was introduced to treated blood samples and allowed to bind to cells at room temperature for 1 h,

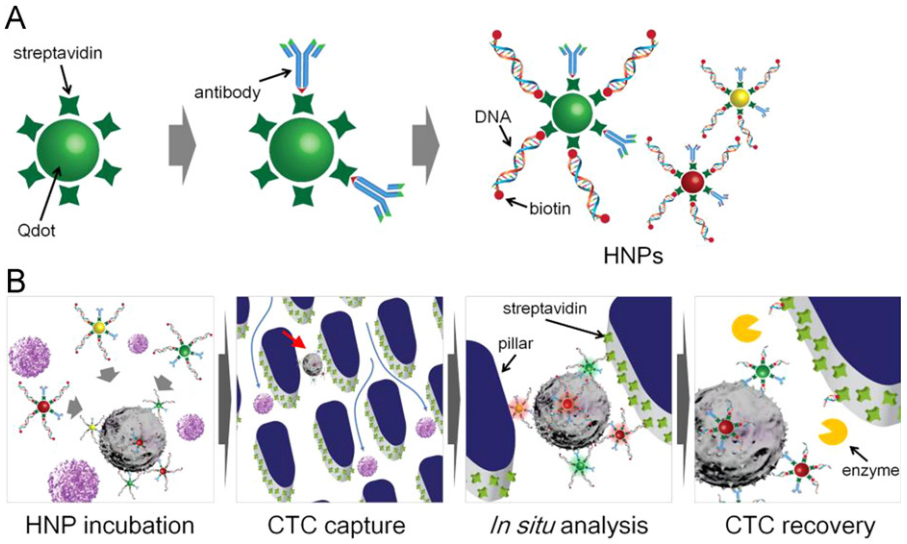


**Fig. 1.** Schematic images of (A) HNP synthesis and (B) CTC capture and *in situ* analysis with capture & recovery chip (CRC) using HNPs. The antibody binds HNP to target cells, while the biotinylated DNA enables the capture of CTC–HNP complex onto streptavidin-coated CRC. Subsequent treatment with restriction enzymes enables the release of CTCs from CRC for collection and further experimentation.

while constantly mixing. After HNP binding, the cell suspension was washed three times with culture media (without serum) by centrifugation (1000 rpm, 3 min) and finally re-suspended in fresh culture media (400 μL), supplemented with 10% FBS. Each sample was injected into CRC at a flow rate of 10 μL/min, and captured cells were subsequently stained with phycoerythrin (PE) conjugated anti-CD45 antibody (BD Biosciences). The chips were subsequently washed with PBS at same flow conditions as before, to remove any unbound materials.

### 2.6. Image acquisition

All images were acquired with an inverted microscope (IX81-ZDC; Olympus) using 20 × objective lens (LUCPlan FLN, NA: 0.45; Olympus, Tokyo, Japan) with a 16-bit monochrome CCD (Orca R2; Hamamatsu photonics, Shizuoka, Japan). Fluorescent images were acquired in three separate channels sequentially to minimize potential cross-talk effect. The entire surface of the chip was scanned using a motorized stage to identify CTCs, based on cell morphology and immunofluorescent staining.

### 2.7. DNA cleavage and release of CTCs

To evaluate the cleavage efficiency of DNA linkers, HNPs were immobilized on streptavidin-coated substrate (Arrayit Co., Sunnyvale, CA) and subsequently treated with a mixture of restriction enzymes, AluI, BamhI, and EcoRI, for 30 min at 37 °C. The release efficiencies of CTCs were calculated as the ratio of number of cells in the capture region before to that after enzyme treatment. Enzyme solutions (500 unit/mL in NE Buffer2) were flowed into the chip at a flow rate of 30 μL/min for 20 min at 37 °C. Released CTCs were trapped in the recovery chamber, and the recovered cells were immediately transferred to a 96-well plate for culturing. Culturing conditions for recovered cells are the same as before.

## 3. Results and discussion

### 3.1. Preparation of hybrid nanoparticles

HNPs were specifically designed to effectively capture CTCs using surface antigens and concurrently analyze expression levels of these

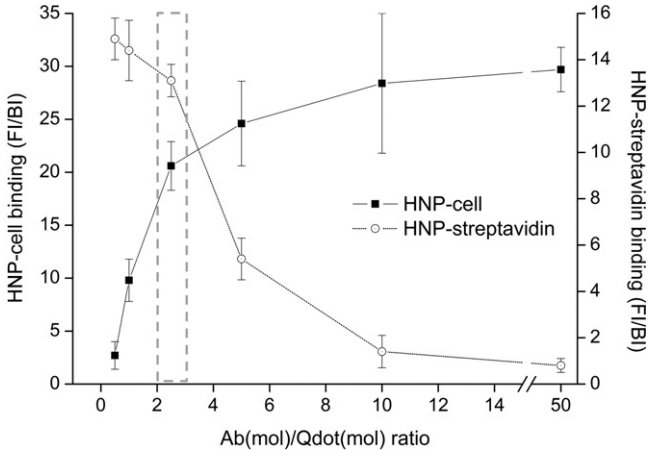


**Fig. 2.** Optimization of HNP synthesis. Double *y*-axis graph shows changes in HNP-to-cell binding (filled squares, left axis) and HNP-to-streptavidin binding (open circles, right axis), both represented by signal intensity (in terms of foreground intensity (FI)/background intensity (BI)) after incubation of cells with HNPs and capturing of cell–HNP complex by streptavidin-coated substrate, respectively.

antigens for possible cancer cell subtyping. For this purpose, each Qdot was conjugated to antibodies for a specific cell surface protein and biotin modified dsDNA with a unique sequence for reversible captured CTCs by streptavidin-coated CRC. For this report, three different HNPs, each with distinct antibodies and dsDNA, were synthesized (HNP A: EpCAM–Qdot(525 nm)–DNA1; HNP B: EGFR–Qdot(565 nm)–DNA2; and HNP C: HER2–Qdot(625 nm)–DNA3).

Performance of HNPs may differ greatly due to the ratio of inputs. Increasing the ratio of antibodies to Qdots will enhance binding of HNPs to target cells, but as there will be less room for dsDNA to bind, capturing of HNP-bound CTCs by CRC may be affected. Thus, it is important to find the optimal ratio of inputs in creating HNPs. For this purpose, we synthesized HNPs at various ratios of antibodies to Qdots. Biotinylated antibodies were introduced to streptavidin-coated Qdots at molar ratios from 0.5:1 to 50:1, as shown in Fig. 2A, since each Qdot has 5–10 streptavidin units immobilized on its surface, and each streptavidin unit is a tetramer, with each subunit binding to biotin with equal affinity. Following this reaction, remaining free streptavidin units were bound to biotin-modified dsDNA.

The binding of antibodies to Qdots was verified by fluorescence microscopy. Tumor cells (SK-BR-3) were incubated with HNPs of different antibody to Qdot ratios, and the average fluorescence intensity in the region of interest (ROI) of these cells was measured. Fluorescence signals were strongly visible ( > 5.0 FI/BI ratio) at antibody to Qdot molar ratio greater than 2.5. To evaluate the binding efficiency of HNPs to streptavidin, HNPs were placed on glass substrates coated with streptavidin arrays, and the fluorescence intensity of HNPs was measured. At antibody to Qdot molar ratio greater than 2.5, the signal intensity decreased sharply, suggesting that HNPs did not bind to glass arrays. Thus, we determined the appropriate molar ratio (antibody:Qdot:DNA = 2.5:1:100) to maximize both antibody capture of cells and HNP immobilization on streptavidin-coated surface.

### 3.2. Classification criteria of cancer cell types

Three types of synthesized HNPs, which were respectively conjugated with anti-EpCAM (green), anti-EGFR (orange), and anti-HER2 (red) antibodies, show different affinities for different breast cancer cell subtypes. EpCAM, which is expressed on the membrane of epithelial cells, but not on hematopoietic cells, is highly expressed in the luminal subtype and weakly expressed in the basal-like subtype. EGFR and HER2, as epidermal growth factor receptors, are often used as therapeutic biomarkers and may be valuable in the clinical setting for personalization of anti-cancer therapy. EGFR is frequently over-expressed in the basal-like subtype. HER2 is expressed in approximately 15–20% of breast cancer patients (Peng and Jordan, 2010).

Three types of cancer cells (MCF-7, SK-BR-3 and MDA-MB-231) were incubated with the three synthesized HNPs, containing antibodies for EpCAM, EGFR, and HER2, respectively. After incubation with HNPs, cells were subsequently stained with Hoechst 33342 (Invitrogen, Carlsbad, CA), which can bind to DNA in live cells. The cells used in this study each have well-known EpCAM, EGFR, and HER2 expression levels: (cell lines: expression levels (EpCAM/EGFR/HER2); MCF-7 (luminal subtype): high/low/low; SK-BR-3 (HER2 subtype): high/high/high; and MDA-MB-231 (basal subtype): low/high/low) (Peng and Jordan, 2010; Prang et al., 2005).

Cells were imaged in bright-field and fluorescence. Cellular expression levels for each protein were calculated by taking the average of foreground intensity within the region of interest (ROI) for a single cell and dividing this value by the average of background intensity in all non-ROI regions of a given image. We determined the appropriate expression level thresholds by its FI/BI ratio and categorized cells into one of four groups: (a) 0 level (FI/BI ratio < 2), (b)+level (2 < FI/BI ratio≤10), (c) ++ level (10 < FI/BI ratio≤20), and (d) +++ level (FI/BI ratio > 20).

Fig. 3 summarizes the results for MCF-7, SK-BR-3, and MDA-MB-231 cells. Different expression levels were found for each surface marker in each cell type: MCF-7—high level of EpCAM (+++), weak level of EGFR (+), and negative HER2; SK-BR-3—high level of EpCAM (+++), moderate level of EGFR (++), and high level of HER2 (+++); and MDA-MB-231—high level of EGFR (+++) and negative EpCAM and HER2.

### 3.3. Design and modeling of capture & recovery chip

The essential parameters that determine the efficiency of CTC capture on CRCs are fluid flow velocity and distance between pillars inside the chip (hereafter referred to as gap distance), as these factors affect the duration and/or chances of cell-to-pillar contact. The CRC chip is composed of separate regions for cell capture and cell recovery (Fig. 4). The capture chamber contains three different sectors with different gap distances (40, 30, and 20 μm in the flow direction), with pillar diameters and gap distances constant within a given sector. Each sector has multiple pillars arranged in a triangular arrangement to maximize capture efficiency. To optimize size and arrangement of these pillars, we performed theoretical analysis of fluid flow path in the capture chamber by simulation. The flow path was considered to be a steady-state problem using fluid flow stream in CFD-ACE+ (ver. 2009, ESI Group, France) with flow rates being increased from 5 to 100 μL/min.

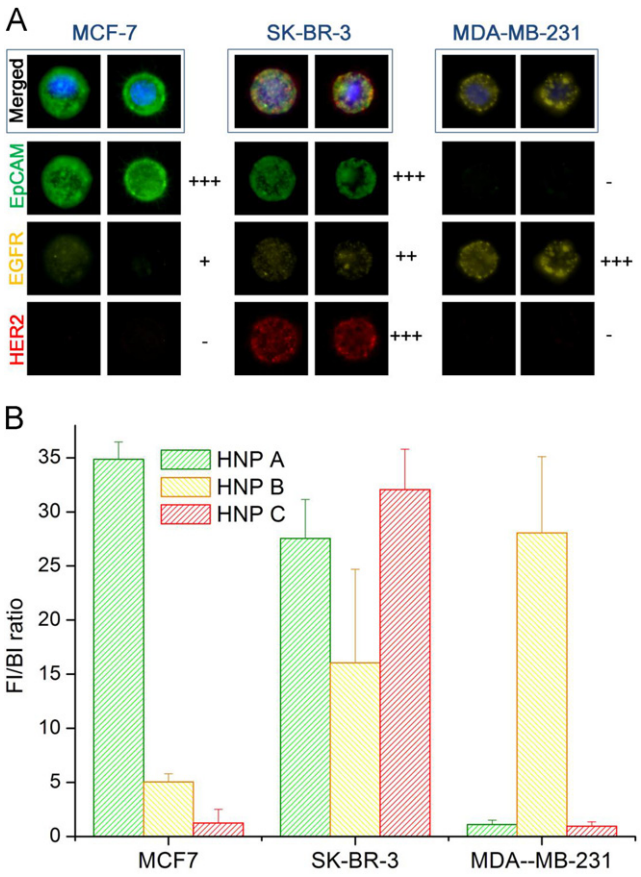


**Fig. 3.** (A) Fluorescence images of three different types of cells (MCF-7, SK-BR-3, and MDA-MB-231) after incubation with all three types of HNPs. (B) Bar graph representing average signal intensity in each of the three channels for each cell–HNP combination shown in (A).

To increase capture performance without causing clogging, gap distances were designed to decrease with each successive sector. The decreased gap distance increases the chance of cell-to-pillar contact. At the same time, as the total volumetric flow rate remains constant, decreased gap distance causes the relative flow velocity to increase, thereby exerting more pressure upon captured cells. However, by increasing the width of the capture chamber toward the outlet, it is possible to maintain the same fluid flow velocity in all sectors.

Fig. 4C shows flow stream displacement in the *x*-direction through the chip for a flow rate of 10 μL/min (chamber depth: 50 μm). Fluid flow velocities were almost evenly distributed along channel. These results also show that fluid flow velocity remained constant within all sectors of the capture chamber, despite having different gap distances (Fig. 4D).

### 3.4. Optimization of the fluidic condition

To evaluate the effect of flow rate on capturing CTCs, SK-BR-3 cells bound with HNPs were placed into PBS at concentration of

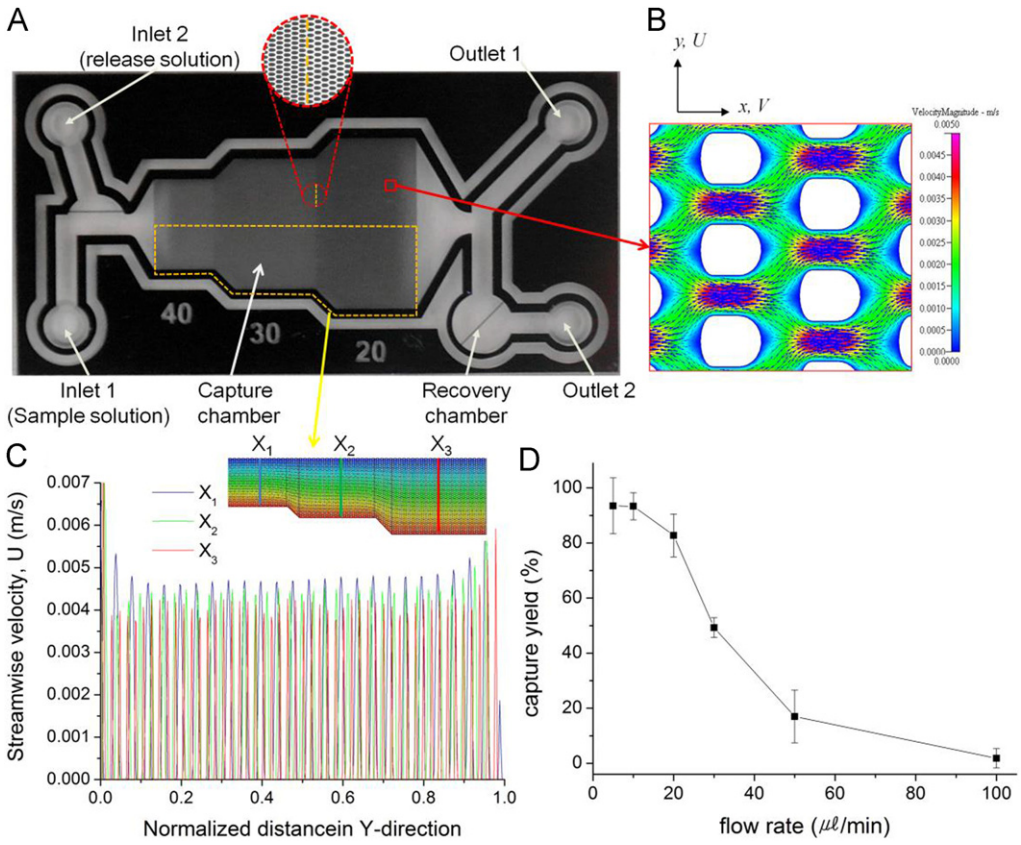


**Fig. 4.** (A) Design of capture & recovery chip (CRC). The capture chamber contains oval shaped micro-pillars arranged in three sectors with different gap distances (40, 30, and 20 μm). (B) Numerical flow simulation data showing distribution of velocities as a contour plot for a small area within the capture chamber. (C) Graph showing streamwise velocities compared for each sector ($X_1$: 40 μm, $X_2$: 30 μm, and $X_3$: 20 μm gap distances) is shown with velocity vector plot (top right) colored by magnitude of velocity. (D) Capture efficiency of CTCs from pre-treated blood samples spiked with 100 tumor cells as a function of flow rate. (For interpretation of the references to color in this figure legend, the reader is referred to the web version of this article.)

100 cells/mL and captured by streptavidin-coated CRC. To investigate whether CTCs were captured non-specifically, either by size or non-specific binding, the capturing efficiencies of HNP-bound cells were compared to uncoated chips. Significant differences could be observed between the two conditions, as cells were visually evident in the chip with streptavidin-coated pillars, while no cells could be identified in chip with uncoated pillars.

HNP-bound cells were flowed through CRC at flow rates ranging from 5 to 100 μL/min, as shown in Fig. 4B. The capture efficiency was greater than 90% at flow rate of 10 μL/min and decreased as the flow rate increased. No improvements could be seen at flow rates lower than 10 μL/min, leading us to select 10 μL/min as the flow rate for subsequent studies.

The spatial distributions of cell capture within the capture chamber were measured for each of the three sectors (with different gap distances). The distribution was as follows: $1.2 \pm 1.7\%$ in sector I (gap: 40 μm), $24.8 \pm 4.8\%$ in sector II (gap: 30 μm), and $74.0 \pm 3.1\%$ in sector III (gap: 20 μm). These results show that most cells were captured at sector III.

### 3.5. Capture and identification of CTCs

Three different breast cancer cells (MCF-7, SK-BR-3, and MDA-MB-231) were used to evaluate HNPs. MCF-7 and MDA-MB-231 cells exhibit high EpCAM and EGFR expression, while SK-BR-3 cells show high EpCAM, HER2, and moderate EGFR expressions. As each HNP has exposed biotin arm that can readily bind to streptavidin-coated pillars in CRC, the capture efficiency depends on the density of biotin in HNP-bound cells. To determine the capture efficiency for each of the three types of cells used in this study, we separately spiked 100 cells of each cell type into 1 mL of pre-treated blood sample, which was subjected to density-gradient centrifugation, resulting in suspension of mostly leukocytes. This mixture was then incubated with HNPs. Next, the cell suspension was flowed through CRC. Captured cells were classified as CTCs or not based on cell morphology and immunofluorescence staining (CD45 negative and positive for specific HNPs, depending on cell type). The capture efficiencies of MCF-7and SK-BR-3 cells were respectively $81.3 \pm 2.3\%$ and $91.2 \pm 8.1\%$ (Fig. 5A). Better performance in capturing SK-BR-3 cells may be due to the greater number of HNPs that bind with these cells compared to MCF-7 cells, as SK-BR-3 cells show greater overall expression level for the three types of antibodies (EpCAM, EGFR, and HER2) used. For MDA-MB-231 cells, which have relatively low surface protein expression compared to the other two cell lines, the capture efficiency was still high ($90.0 \pm 7.1\%$). This high efficiency may be due to the larger diameter of MDA-MB-231 cells compared to other cells (Fig. S3 of Supplementary data shows the size distribution of cells used in this study), allowing for higher chance of contact with the streptavidin-coated pillars. Taking data from all three cancer cell lines together, the average capture efficiency of cells was 87.5%. As for identification of breast cancer cell subtypes, based on different surface protein expressions, captured cells were successfully identified by different signal intensities generated by HNPs for each of the three antigens considered. The overall identification accuracy was 92.4% (MCF-7: 94.7%; SK-BR-3: 99.3%; and MDA-MB-231: 83.3% of captured cells).

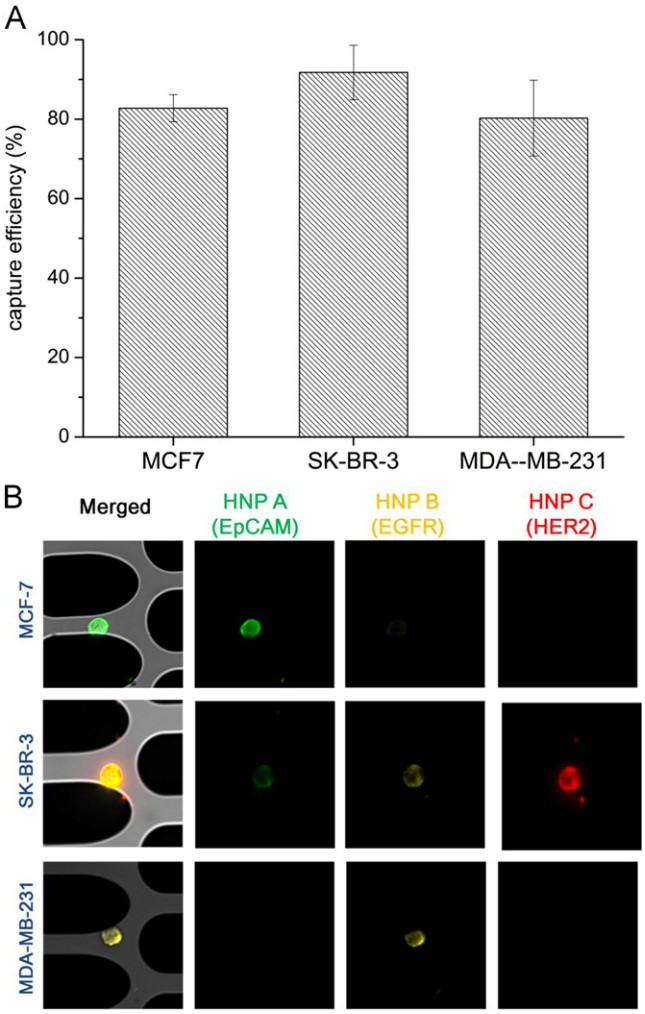


**Fig. 5.** CTC capture and identification. (A) Capture efficiency for each of the cell line tested (MCF-7, SK-BR-3, and MDA-MB-231). Samples were generated from pre-treated blood samples spiked with 100 tumor cells and flown through CRC. (B) Fluorescence images of CTCs captured by the micro-pillar array of CRC.

### 3.6. Recovery and culture of captured CTCs

Cells captured by CRC were released by treatment with restriction enzymes, followed by microfluidic flow to transport these released cells to the recovery chamber of the chip. As each cell is connected to the chip surface by biotin, which itself is connected to the rest of HNP structure by a specific dsDNA sequence, it is possible to release cells that express a specific antigen only by using specific restriction enzymes. The condition required to effectively cleave DNA linkers was calculated to be 500 unit/mL of restriction enzyme for 20 min at 37 °C, and subsequent tests with all three types of HNPs—each with unique DNA sequence—showed that more than 94% of initially attached HNPs were specifically released after each enzyme treatment (Fig. 6A). All subsequent DNA cleavages reported in this paper were performed with the condition aforementioned.

This process was verified for captured CTCs inside CRC, as shown in Fig. 6B. To verify if it is possible to release cells based on their phenotype, MCF-7 cells, which have high EpCAM and weak EGFR expression levels, were treated with AluI and EcoRI; SK-BR-3 cells with significant expression levels of three protein markers, EpCAM, EGFR and HER2, were treated with mixture of all three enzymes, and MDA-MB-231, expressing only EGFR, was treated with EcoRI. The release efficiencies of the cells were correspondingly 78.6%, 93.7% and 86.0%. To fully evaluate the possibility of selective recovery using our approach, we compared release efficiencies among captured tumor cells. In case of AluI treatment, with MCF-7 cells as the main target, the percentage of putative MCF-7 cells among all released cells was 66.7%. Similarly, MDA-MB-231 was recovered with 61.8% purity through EcoRI treatment (Fig. S4 of Supplementary data). To demonstrate cellular viability post-isolation using HNPs, recovered cells were collected from the recovery chamber, transferred to a 96-well plate, and cultured *in vitro*. Cells adhered and proliferated, forming colonies as time passed (Fig. S5 of Supplementary data). These results suggest that CTCs could be selectively recovered from the chip, without affecting their viability or proliferative capacity.

## 4. Conclusion

This study demonstrates the successful synthesis and application of hybrid nanoparticles (HNPs), which consist of specific antibodies and biotin-conjugated DNAs attached to quantum dots, to perform simultaneous capture, enumeration, and identification of CTCs by phenotype (based on *in situ* protein expression), without affecting cellular viability. Using HNPs, we aimed to achieve three primary goals: (a) increase capture efficiency of tumor cells from blood; (b) allow accurate quantification of protein expression for each individual cell to provide more clinical information toward personalized therapy; and (c) enable the culturing of these captured cells *in vitro* to study additional information, such as drug suitability. To increase CTC capture efficiency, we used not only antibodies to EpCAM but also EGFR and HER2 to capture CTCs with low EpCAM expression. Some breast cancer cells, such as those of the basal subtype, express low levels of EpCAM. Moreover, CTCs are believed to have undergone EMT and, thus, lack or only weakly express EpCAM. Therefore, using only EpCAM-based capture techniques, which is popular in many reported CTC capture methods, could lead to failure in detecting CTC populations that have undergone EMT (Cancer Discovery, December 2011 1, 580; BMC Cancer, 2012, 12, 178).

Using three different HNPs, each for one of the three proteins aforementioned, we were able to successfully capture tumor cells onto an in-house developed chip, which was specifically designed to effectively capture and make visualization by microscopy easier. Our approach showed an average CTC capture efficiency of 87.5%, including 90.0% of MDA-MB-231 cells, which are EpCAM negative cells that were captured. Furthermore, using HNPs, these captured cells could simultaneously be identified by their *in situ* protein expression. Following image analysis, we were able to assess the expression levels of each surface protein for each captured cell. Using classification criteria developed in this paper, the identification accuracy was 92.4%. These results demonstrate that HNP binding provides not only high capture efficiency of CTCs but also enables simultaneous phenotype assessment of captured CTCs.

As culture of recovered CTCs could lead to better clinical decision, with more information for assessment of cancer prognosis and prediction of potential responses to targeted therapies available, we developed a novel approach to recover captured cells from the capture chamber, using HNPs with specific recognition DNA sequences, acting as a linker between the chip and the rest of HNP–cell complex. Following restriction enzyme treatment, cells were easily released from the capture chamber, without exposure to harsh conditions, such as low pH or high temperature, which may affect cellular viability. To demonstrate the release and recovery of captured cells, we applied suitable restriction enzymes for each cell type, based on phenotype classification. This enables the selective recovery of only desired cells from a larger pool of captured cells.

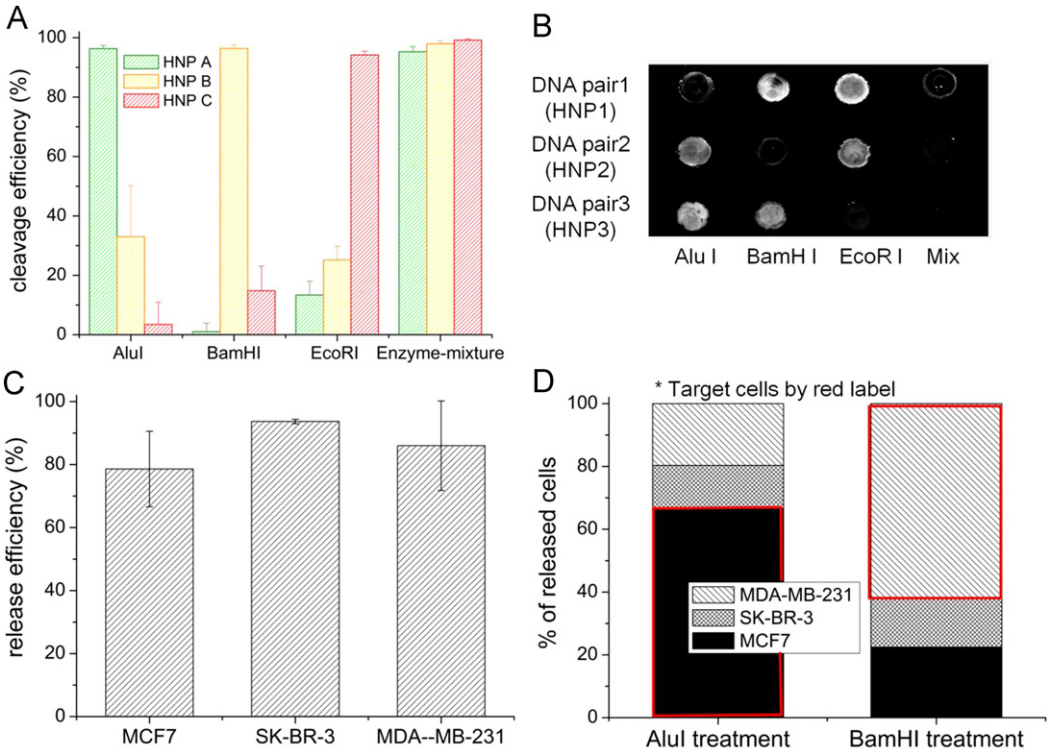


**Fig. 6.** Cleavage of DNA linker and subsequent release of captured CTCs. (A) Cleavage efficiency of DNA linkers on HNPs using three different restriction enzymes (AluI, Bam*HI*, and Eco*RI*). HNPs immobilized on streptavidin-coated substrate were used to calculate cleavage efficiencies. (B) Release efficiency of captured CTCs after treatment with restriction enzymes. (C) Component ratio of cells released after treatment with a particular restriction enzyme.

Moreover, *in vitro* culture of recovered cells proved that the entire capture and recovery process did not affect cell viability or proliferative capacity. CTC recovery by HNP has several advantages over conventional CTC detection methods: it is possible to (a) efficiently capture heterogeneous CTCs, including those with either high or low EpCAM expression; (b) identify cell subtype simultaneously through analysis of *in situ* protein expression, using the same surface antigens used for capture; (c) recover these captured CTCs in their intact and native form; (d) selectively recover the wanted cells; and (e) culture them *in vitro*, enabling additional studies, such as drug screening.

## Acknowledgments

We would like to thank all volunteers who contributed blood samples, thereby enabling this research. H.Y. Cho and J.W. Choi were supported by National Research Foundation of Korea (NRF) grant funded by the Korea government (MEST) (2009-0080860).

## Appendix A. Supporting information

Supplementary data associated with this article can be found in the online version at http://dx.doi.org/10.1016/j.bios.2013.03.040.

## References

Bednarz-Knoll, N., et al., 2011. Breast Cancer Research 13 (6), 228.
Chung, Y.K., et al., 2011. Biosensors and Bioelectronics 26 (5), 2520–2526.
Cohen, S.J., et al., 2008. Journal of Clinical Oncology 26 (19), 3213–3221.
Gerges, N., Rak, J., Jabado, N., 2010. British Medical Bulletin 94, 49–64.
Goldhirsch, A., et al., 2011. Annals of Oncology 22 (8), 1736–1747.
Gorges, T.M., et al., 2012. BMC Cancer 12, 178.
Ignatiadis, M., Reinholz, M., 2011. Breast Cancer Research 13 (5), 222.
Kirby, B.J., et al., 2012. PLoS One 7 (4), e35976.
Kumeria, T., et al., 2012. Biosensors and Bioelectronics 35 (1), 167–173.
Lazar, D.C., et al., 2012. Physical Biology 9 (1), 016002.
Lee, H.J., et al., 2009. Biosensors and Bioelectronics 24 (10), 3120–3125.
Lin, C.W., et al., 2012. Journal of Biological Chemistry 287 (47), 39449–39459.
Lin, H., et al., 2011. Critical Reviews in Oncology/Hematology 77 (1), 1–11.
Nagrath, S., et al., 2007. Nature 450 (7173), 1235–1239.
Pantel, K., Alix-Panabières, C., 2010. Trends in Molecular Medicine 16 (9), 398–406.
Paterlini-Brechot, P., Benali, N.L., 2007. Cancer Letters 253 (2), 180–204.
Peng, J., Jordan, V.C., 2010. International Journal of Oncology 36 (2), 451–458.
Prang, N., et al., 2005. British Journal of Cancer 92 (2), 342–349.
Punnoose, E.A., et al., 2010. PLoS One 5 (9), e12517.
Riethdorf, S., et al., 2010. Clinical Cancer Research 16 (9), 2634–2645.
Sieuwerts, A.M., et al., 2009. Journal of the National Cancer Institute 101 (1), 61–66.
Sihto, H., et al., 2011. Breast Cancer Research 13 (5), R87.
Talasaz, A.H., et al., 2009. Proceedings of the National Academy of Sciences of the United States of America 106 (10), 3970–3975.
Yu, M., et al., 2011. Journal of Cell Biology 192 (3), 373–382.
Zylstra, J., et al., 2012. Tailoring quantum dot interfaces for improved biofunctionality and energy transfer, In: Hepel, M., Zhong, C.J. (Eds.), Functional Nanoparticles for Bioanalysis, Nanomedicine and Bioelectronic Devices, vol. 1, ACS Symposium Series, vol. 1112, Oxford University Press, Oxford, pp. 212–245.